AGU PUBLICATIONS

JGR

Journal of Geophysical Research: Atmospheres

RESEARCH ARTICLE
10.1002/2017JD026953

Key Points:
- The impact of meridional structures of tropical SST on the Hadley circulation (HC) is quantitatively evaluated during the seasonal cycle
- The amplitude of the HC response to the equatorially asymmetric SST is four times than that of the equatorially symmetric SST
- The NCEP1 reanalysis shows limitations in depicting the seasonal cycle of the equatorially symmetric variations of the HC

Correspondence to:
J. Li,
ljp@bnu.edu.cn

Citation:
Feng, J., J. Li, F. Jin, S. Zhao, and F. Xie (2017), The responses of the Hadley circulation to different meridional SST structures in the seasonal cycle, *J. Geophys. Res. Atmos.*, *122*, 7785–7799, doi:10.1002/2017JD026953.

Received 14 APR 2017
Accepted 18 JUL 2017
Accepted article online 21 JUL 2017
Published online 3 AUG 2017

The responses of the Hadley circulation to different meridional SST structures in the seasonal cycle

Juan Feng[1], Jianping Li[1,2], Feifei Jin[3], Sen Zhao[3,4], and Fei Xie[1]

[1]State Key Laboratory of Earth Surface Processes and Resource Ecology and College of Global Change and Earth System Science, Beijing Normal University, Beijing, China, [2]Laboratory for Regional Oceanography and Numerical Modeling, Qingdao National Laboratory for Marine Science and Technology, Qingdao, China, [3]School of Ocean and Earth Science and Technology, University of Hawaii, Honolulu, Hawaii, USA, [4]Key Laboratory of Meteorological Disaster of Ministry of Education, College of Atmospheric Science, Nanjing University of Information Science and Technology, Nanjing, China

Abstract The meridional structure of sea surface temperature (SST) plays an important role in determining the variations of the Hadley circulation (HC). The quantitative differences in the HC caused by the changing meridional structures of SST over seasonal cycles remain unclear. To determine the quantitative response of the HC to the meridional structure of SST during the seasonal cycle, this study decomposes the variations of the SST and HC into two components: equatorially asymmetric components (i.e., SEA for SST and HEA for HC) and equatorially symmetric components (i.e., SES for SST and HES for HC). Variations in HEA (HES) are closely associated with those in SEA (SES). In this study, five atmospheric reanalyses and two SST reanalyses are analyzed, focusing on the period of 1979–2013. The response amplitude of HEA to SEA is about four times than that of HES to SES in most of the reanalyses. This result provides a possible explanation for the dominance of the equatorially asymmetric mode over the variability of the HC during the seasonal march.

1. Introduction

The Hadley circulation (HC) is a large-scale thermally direct meridional overturning extending from the equator to about 30° latitude in each hemisphere with seasonally migrating poleward boundaries [*Quan et al.*, 2004]. It bridges the tropics and higher latitudes via heat and momentum transport by mean flows and eddies [*Lindzen*, 1994; *Hou*, 1998] and therefore plays an important role in global climate system [*Peixoto and Oort*, 1992; *Diaz and Bradley*, 2004; *Seidel et al.*, 2007; *Feng et al.*, 2013; *Su et al.*, 2014]. Previous studies have focused on two key aspects of the HC: first, changes in the HC itself, including the intensity and extent, and second, the long-term variability and climatic impacts. As to the variation of its intensity, although consistent results suggest a tendency toward intensification in both the National Centers for Environmental Prediction-National Center for Atmospheric Research Global Reanalysis (NCEP1) data set [*Quan et al.*, 2004; *Ma and Li*, 2008] and the 40 year European Centre for Medium-Range Weather Forecasts Re-Analysis (ERA-40) data set [*Mitas and Clement*, 2005] throughout their periods, the intensity trends are generally inconsistent among the data sets [*Nguyen et al.*, 2013]. No discernible intensification trend can be detected based on rawinsonde observations and the National Centers for Environmental Prediction-Department of Energy (NCEP2) Atmospheric Model Intercomparison Project reanalysis over its period [*Mitas and Clement*, 2005].

Regarding the extent of the HC, since *Fu et al.* [2006] demonstrated that the extent of the HC shifted poleward by approximately 2° in latitude over the period 1979–2005, other studies based on various data sets have further evaluated the variations in the extent of the HC during different seasons and have confirmed the expansion of the HC [e.g., *Fu et al.*, 2006; *Hu and Fu*, 2007; *Previdi and Liepert*, 2007; *Seidel and Randel*, 2007; *Johanson and Fu*, 2009; *Stachnik and Schumacher*, 2011]. Although different data sets show differences in the scale of the expansion, consistent results have demonstrated that the expansion is most pronounced during boreal summer and autumn [*Nguyen et al.*, 2013] and that the extent of HC expansion during different seasons based on the various data sets is within the range 1.21° to 5° of latitude [e.g., *Hudson et al.*, 2006; *Johanson and Fu*, 2009]. In addition, the variations in the ascending branch of the HC are explored in recent studies. The seasonal shift of the ascending branch of the HC is explored [*Feng et al.*, 2016a]. As to its long-term variation, it is shown that the ascending branch of the HC becomes narrower in response to surface warming [*Byrne and Schneider*, 2016; *Wodzicki and Rapp*, 2016]. And the narrowed variation of the HC's ascent differs greatly among climate models and may has profound implications for global hydrological sensitivity [*Su et al.*, 2017].

The long-term variability of the HC, as well as its climatic impacts, have also received considerable attention. In particular, empirical orthogonal function (EOF) analysis has been used to detect the temporal and spatial characteristics of the HC related to both its annual and long-term seasonal variability. For example, *Dima and Wallace* [2003] indicated that the seasonal cycle of the HC is dominated by two components of comparable mean-square amplitude: the equatorially symmetric component that shows little seasonal variation and the equatorially asymmetric component that varies sinusoidally with the seasons. For the long-term interannual variability, *Ma and Li* [2008] found that the boreal winter HC is dominated by two principal modes: an equatorially asymmetric and an equatorially symmetric mode. A similar result has also been found for the boreal summer HC [*Feng et al.*, 2011]. It has been shown that the variation of the asymmetric mode is connected to the sea surface temperature (SST) over the Indo-Pacific region, whereas the variation of the equatorially symmetric mode is linked to SST over the tropical Pacific in both the boreal winter [*Ma and Li*, 2008] and summer [*Feng et al.*, 2011]. *Feng et al.* [2013] and *Guo et al.* [2016] also reported similar equatorially asymmetric and symmetric modes during the boreal spring and autumn HC. *Feng et al.* [2013] illustrated how the inhomogeneous warming of SST over the tropical oceans would alter the meridional gradient of SST, and so contribute to the formation of the equatorially asymmetric mode. This helps to identify the factors controlling the variations of the equatorially asymmetric mode in both the boreal winter and summer [*Li and Feng*, 2017]. These studies have emphasized the important role of the meridional structure of SST in influencing variations of the HC.

In addition, other studies have used theoretical analysis and models to demonstrate the considerable impact of the meridional gradient of the underlying thermal conditions on the HC. Result of a theoretical model of the boundary layer has shown that adjusting the meridional structure of tropical SST can change the position and strength of the convergence [*Schneider and Lindzen*, 1977; *Rind and Rossow*, 1984; *Lindzen and Nigam*, 1987] and influence the vertical motion in the lower troposphere [*Lindzen and Hou*, 1988; *Hou and Lindzen*, 1992]. Furthermore, the meridional gradient of SST has a significant impact on the convergent flow in the planetary boundary layer and the near-neutral stratification of the atmosphere [*Numaguti*, 1994]. On the other hand, it is reported that the response of both dry [*Plumb and Hou*, 1992] and moist [*Zheng*, 1998] atmosphere to a subtropical thermal forcing exhibit threshold behavior; for example, a supercritical forcing could induce a strong meridional circulation. And it is found that the HC dominantly adopts the angular momentum conservation regime during solstice seasons (i.e., being equatorially asymmetric) and the eddy-mediated regime (i.e., being equatorially symmetric) during equinox seasons [*Walker and Schneider*, 2005, 2006; *Schneider and Bordoni*, 2008; *Bordoni and Schneider*, 2010]. In addition, *Melice and Servain* [2003] showed that the regional meridional SST gradient within the tropical Atlantic has a significant influence on sea level pressure and regional circulation anomalies. These research studies emphasized the effect of the meridional structure of SST on the HC, mainly on its intensity. Recently, *Adam et al.* [2014] have shown that the widening of the HC from 1997 to 2012 was associated with a decreased meridional gradient of SST between the tropics and midlatitudes. Nevertheless, these previous studies qualitatively highlighted the important role of the meridional structure of the underlying thermal conditions on the HC; however, the exact differences between the responses of the HC to different meridional thermal conditions remain to be quantified. A recent work has quantitatively assessed the response of the HC to different SST meridional structures focused on the interannual scale [*Feng et al.*, 2016b]. It is found that the responses of the HC to the equatorially asymmetric SST are approximately five times than that of the equatorially symmetric SST [*Feng et al.*, 2016b]. In this study, we further examine the differences in the response of the HC to differing SST meridional structures but focus on the seasonal cycle. We also investigate whether the response of the HC to different meridional thermal structures is sensitive to the timescale, noting that the dominant mode of the HC in the seasonal cycle and long-term seasonal trends shows certain differences [*Dima and Wallace*, 2003; *Feng et al.*, 2013].

In this study, the variations of the underlying thermal conditions (e.g., SST) and of the HC were physically separated into two components (i.e., the equatorially asymmetric and symmetric parts) to compare their different impacts. The remainder of this paper is organized as follows. Section 2 describes the data sets and methodology. The climatological characteristics of the HC and zonal mean SST over the seasonal cycle are illustrated in section 3. Section 4 demonstrates the responses of the HC to the different SST meridional structures found in the various reanalysis data sets. Section 5 compares the differences of the

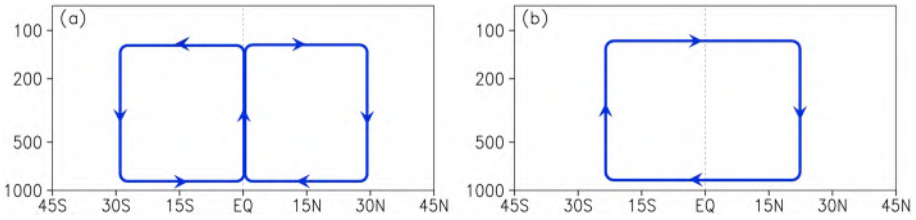

Figure 1. Schematic diagrams showing the (a) equatorially symmetric component and (b) equatorially asymmetric component of the HC. The blue arrows represent the direction of the circulation.

responses over different timescale, i.e., the seasonal cycle versus interannual. Finally, section 6 contains a short discussion and our conclusions.

2. Data Sets and Methodology

2.1. Data Sets

Five atmospheric and two SST reanalysis data sets were used in this study to objectively estimate the response of the HC to different SST meridional structures. These widely used data sets were NCEP1 covering the period 1948 to present [*Kalnay et al.*, 1996], NCEP2 Atmospheric Model Intercomparison Project reanalysis covering the period 1979 to the present [*Kanamitsu et al.*, 2002], the European Centre for Medium-Range Weather Forecasts Re-Analysis (ERA) interim globally archived data set that covers 1979 to the present [*Dee et al.*, 2011], the Japanese reanalysis data set (JRA) that covers 1979 to the present [*Onogi et al.*, 2005], and the recently released NCEP Climate Forecast System Reanalysis (CFSR) that covers the period of 1979–2010 [*Saha et al.*, 2010]. The NCEP1, NCEP2, and CFSR data sets have a horizontal resolution of 2.5° × 2.5°, and the ERA and JRA data sets have a horizontal resolution of 1.5° × 1.5° and 1.25° × 1.25°, respectively. Multireanalyses are used to verify that the reliability of the result is due to that SST data sets used as boundary forcing for the atmospheric reanalyses are different, which may has a potential role in impacting the air-sea interaction [*Parfitt et al.*, 2017].

The global SST reanalysis data sets used to analyze the meridional SST features over the seasonal cycle were the UK Met Office Hadley Centres Sea Ice and SST data set (HadISST) on a 1° × 1° resolution [*Rayner et al.*, 2003] and the Extended Reconstructed SST (ERSST) version 3 on a 2° × 2° grid [*Smith et al.*, 2008]. Here the common available period of 1979–2013 was used as the climatological mean for most of the analysis except for the CFSR, which is only available between 1979 and 2010.

2.2. Methodology

The mass stream function (MSF, ψ) of the mean meridional circulation was used to characterize the HC. Clockwise vertical circulation (the northern cell) is defined as positive and anticlockwise vertical circulation (the southern cell) is defined as negative [*Holton*, 1994]. That is, the sign of the MSF in the Southern Hemisphere (SH) is the opposite of that in the Northern Hemisphere (NH). Note that the ψ is a two-dimensional variable, containing information in both the meridional (i.e., v) and vertical (i.e., ω) directions, and the value of ψ includes both the magnitude and direction of the HC.

To examine the possible impacts of the different meridional distributions of tropical SST on the HC, the spatial variations in SST and HC were separated into two components, i.e., the equatorially asymmetric component and the equatorially symmetric component. For a one-dimensional variable f, the equatorially symmetric (fs) and asymmetric (fa) variations can be decomposed as follows:

$$fs(y) = \frac{f(y) + f(-y)}{2}, \quad fa(y) = \frac{f(y) - f(-y)}{2} \tag{1}$$

where y corresponds to the equatorially symmetric meridional locations. Note that the sum of fs and fa is equal to the original f. For a one-dimensional variable (e.g., zonal mean SST), it is obtained that

$$fs(y) = fs(-y), \quad fa(y) = -fa(-y) \tag{2}$$

However, it is not the case for MSF since it is a two-dimensional variable. A schematic representation of the equatorially symmetric and asymmetric variations of the HC is shown in Figure 1. For the equatorially symmetric component of the HC, the northern and southern cells of the HC are mirrored over the equator. The southern and northern cells share a combined ascending branch located at the equator, with separated descending branches in the subtropical regions of the two hemispheres (Figure 1a). That is,

$$v(y) = -v(-y), \quad \omega(y) = \omega(-y), \quad \psi(y) = -\psi(-y) \tag{3}$$

for the equatorially symmetric component of HC. However, the ascending branch is located in the SH for the equatorially asymmetric component of the HC (Figure 1b), with opposite vertical motion in the two hemispheres in the tropics, i.e., ascending in the tropical SH but descending in the tropical NH. That is,

$$v(y) = v(-y), \quad \omega(y) = -\omega(-y), \quad \psi(y) = \psi(-y), \tag{4}$$

for the equatorially asymmetric component of HC.

As the zonal mean SST is a one-dimensional variable, the equatorially symmetric variations take the form of a parabolic variation centered on the equator, however, with contrary characteristics within the tropics for the equatorially asymmetric component, i.e., with positive values in the SH but negative in the NH, in contrast with same abstract values (figure not shown).

Following the above considerations, the equatorially asymmetric component of the HC (i.e., HEA) and the equatorially symmetric variations of the HC (i.e., HES) can be obtained by following *Feng et al.* [2016b]:

$$\mathrm{HEA}(j) = \frac{\mathrm{MSF}(j) + \mathrm{MSF}(-j)}{2}, \ \mathrm{HES}(j) = \frac{\mathrm{MSF}(j) - \mathrm{MSF}(-j)}{2}. \tag{5}$$

As for SST, the equatorially asymmetric (i.e., SEA) and equatorially symmetric (i.e., SES) variations are defined as

$$\mathrm{SEA}(j) = \frac{\mathrm{SST}(j) - \mathrm{SST}(-j)}{2}, \ \mathrm{SES}(j) = \frac{\mathrm{SST}(j) + \mathrm{SST}(-j)}{2}, \tag{6}$$

where j and $-j$ correspond to the equatorially symmetric meridional locations of the grid points.

EOF analysis was used to detect the leading mode of the variations of SST and the HC during the seasonal cycle after removing the annual mean. The relationship between the HC and SST was investigated using correlation analysis. Spatial correlation was used to examine the similarity of the two variables in the spatial distributions. The regression was calculated using least squares linear regression. The statistical significance of the correlation and regression values was evaluated by means of a two-sided Student's t test.

3. Climatological Characteristics Over the Seasonal Cycle

3.1. Hadley Circulation

The climatological annual mean MSF, as well as EOF1 over the seasonal cycle, based on the five reanalysis data sets are shown in Figure 2. The five reanalyses are highly consistent with each other. The southern and northern cells of the HC are of the same magnitude and extent and lie between approximately 30°S and 30°N. The combined upward branch is located to the north of the equator (Figures 2a–2e), and this is consistent with the annual mean position of the Intertropical Convergence Zone also being located north of the equator [*An et al.*, 2015]. An equatorially asymmetric circulation dominates the variability of the seasonal cycle of the HC and explains about 97% of the variance. The stronger component of this mode extends from 20°S to 30°N and is centered to the north of the equator, with the ascending branch located at about 20°S and the descending branch around 30°N. The southern counterpart of this mode is much weaker and covers approximately 15° of latitude. The descending branch of this component is located to the south of 30°S. The second mode of the seasonal cycle of the HC is equatorially symmetric and explains about 2% of

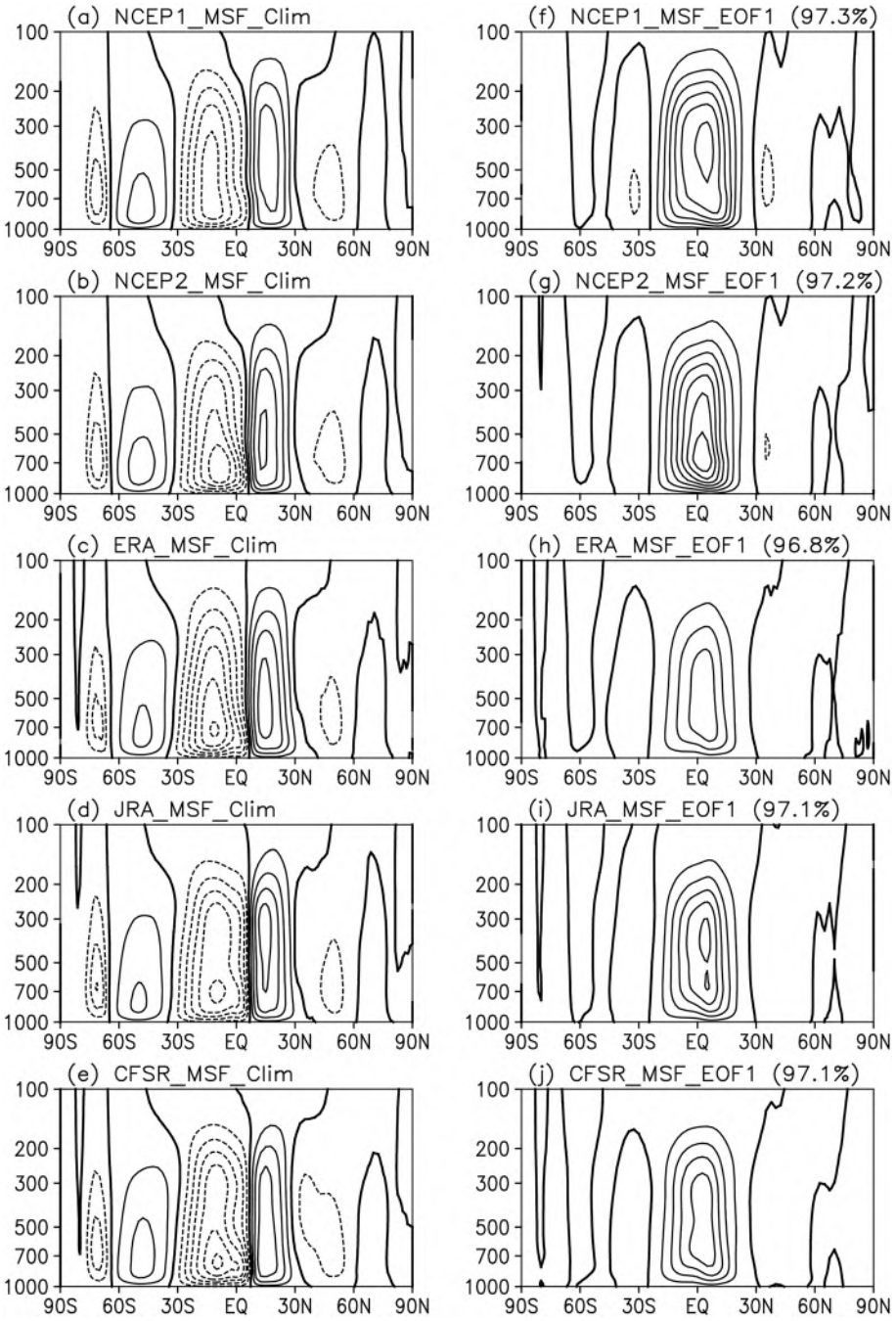

Figure 2. Climatological annual mean MSF based on the (a) NCEP1, (b) NCEP2, (c) ERA, (d) JRA, and (e) CFSR reanalyses, respectively. The contour interval is 0.03×10^{10} kg/s. The solid (dotted) contours are positive (negative). (f–j) As in Figures 2a–2e but for the principal mode of the HC during the seasonal cycle.

the variance across the various reanalyses (figure not shown). As this second mode explains little of the variance, it is not considered further in this study.

The principal component (PC) of EOF1 shows a sinusoidal variation along the seasonal march (Figure 3), with positive values during the boreal winter half-year (November to April) and negative values during the summer half-year (May to October). This sinusoidal variation is consistently observed in the five reanalyses, highlighting the reliability of the result. Note that our results agree with *Dima and Wallace* [2003], and the

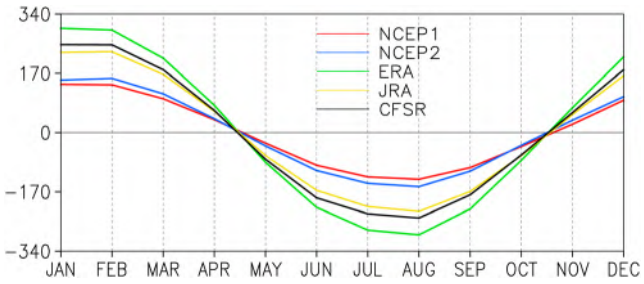

Figure 3. Time series of EOF1 of HC during the seasonal cycle based on the NCEP1 (red), NCEP2 (blue), ERA (green), JRA (yellow), and CFSR (black) reanalyses, respectively.

spatial distribution of this mode is similar to the EOF1 of the long-term variability of the seasonal HC [e.g., *Ma and Li*, 2008; *Feng et al.*, 2013; *Guo et al.*, 2016]. However, this equatorially asymmetric mode accounts for an even larger proportion of the variance during the seasonal cycle than was reported by *Dima and Wallace* [2003] and also more than in the seasonal variability of the HC [e.g., *Feng et al.*, 2013].

3.2. Tropical Zonal Mean SST

The climatological distribution of zonal mean SST within the tropics, and its principal mode, as well as the PC based on the ERSST and HadISST data sets during the seasonal cycle, is shown in Figure 4. Although the exact values and amplitudes of the two reanalyses show small differences, the spatial distribution and structure based on the two reanalyses are highly consistent with each other. The zonal mean tropical SST displays a bimodal structure that is mirrored at around 5° latitude in each hemisphere. The peak value in the SH is smaller than that in the NH. This supports the location of the ascending branch of the HC in the climatology being located to the north of the equator (Figure 2). EOF1 of zonal mean SST has an equatorially asymmetric structure and follows an approximately linear change from the SH to the NH (Figure 4b). The PC of this mode shows similar sinusoidal variations to the seasonal cycle, being positive from December to May and negative from June to November (Figure 4c). The transition point of the PC from positive to negative is 1 month later than that of the seasonal cycle of the HC, and this is because the heat capacity of the ocean is greater than that of the land, which leads to faster heating over land than over oceans.

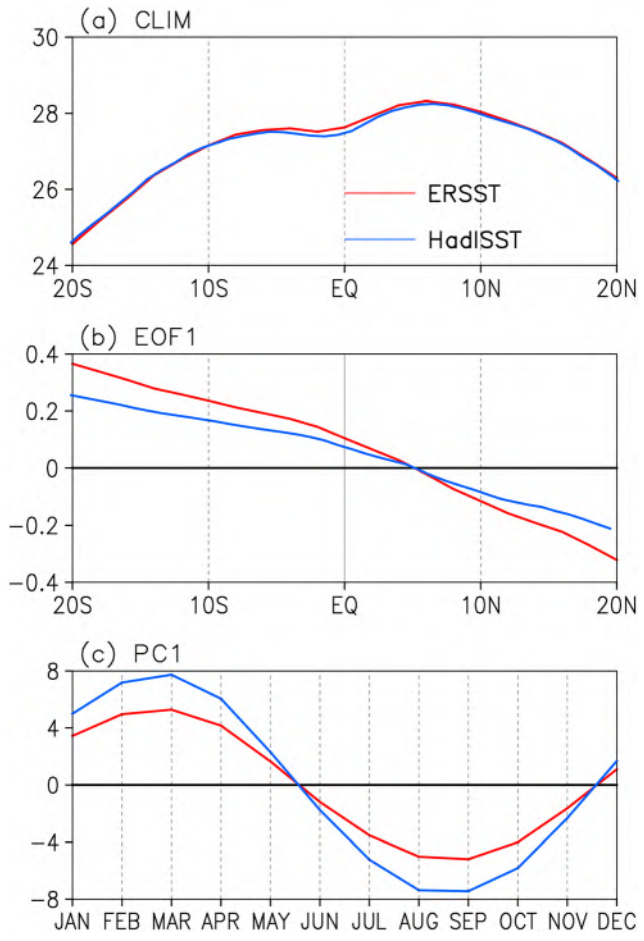

Figure 4. (a) Climatological annual mean of zonal mean tropical SST based on ERSST (red) and HadISST (blue) (°C), respectively. (b) As in Figure 4a but for the EOF1 of zonal mean tropical SST during the seasonal cycle (°C). (c) As in Figure 4a but for the time series of EOF1 of zonal mean SST during the seasonal cycle.

As the variations of the HC are closely linked to the underlying thermal conditions, we also examined the possible linkage between the zonal mean SST and HC during the seasonal march. The correlation coefficient between the PCs of their first principal modes was approximately 0.8 in all five reanalyses, indicating that the seasonal march of the HC is closely associated with that of the tropical SST.

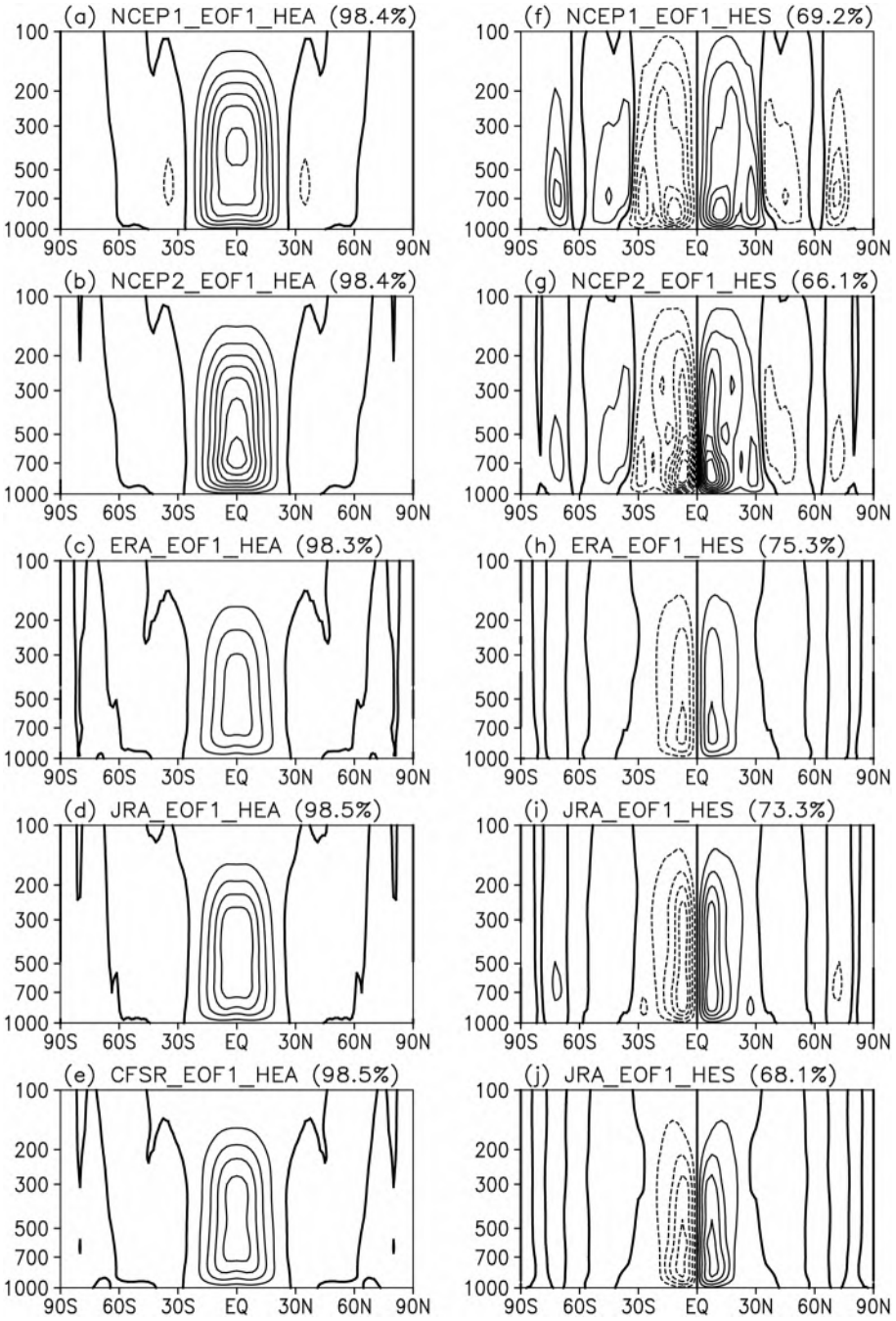

Figure 5. EOF1 of the equatorially asymmetric part of the HC during the seasonal cycle based on the (a) NCEP1, (b) NCEP2, (c) ERA, (d) JRA, and (e) CFSR reanalyses, respectively. The contour interval is 0.02×10^{10}kg/s. The solid (dotted) contours are positive (negative). (f–j) As in Figures 5a–5e but for the first principal mode of the equatorially symmetric part of the HC.

4. Differences in the Response of the HC to SST Between the Equatorially Asymmetric and Symmetric Variations

Using the method described in section 2.2, we decomposed the variation of the HC into two components and then examined the spatial and temporal characteristics of HEA and HES during the seasonal cycle. EOF1 of the HEA and HES is presented in Figure 5. We see that EOF1 of HEA is dominated by an equatorially asymmetric cell, with a combined ascending branch in the SH around 30°S and the descending branch in the NH around

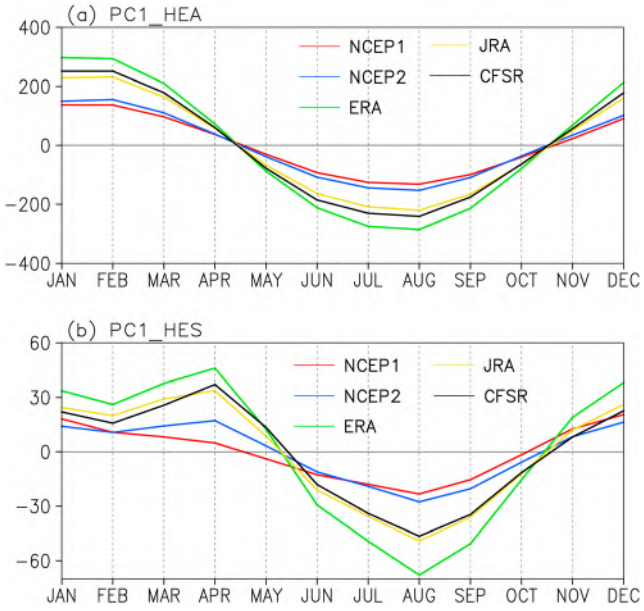

Figure 6. (a) Time series of EOF1 of the equatorially asymmetric part of the HC based on the NCEP1 (red), NCEP2 (blue), ERA (green), JRA (yellow), and CFSR (black) reanalyses, respectively. (b) As in Figure 6a but for EOF1 of the equatorially symmetric part of the HC.

30°N. This mode explains about 98% of the variance across the different reanalyses. We see that the five reanalyses agree well in depicting the intensity, explained variance, and spatial distribution of HEA. The mode of HEA is similar to the mode of the climatological HC, with a high spatial correlation of about 0.98. The PC of this mode also resembles the PC of the climatological HC, showing a correlation of 0.99 (Figure 6a), which suggests that the variation of the HC during the seasonal cycle is derived mainly from the HEA component. This point is consistent with the dominant mode of the HC being equatorially asymmetric.

With respect to the HES component, the dominant mode of HES presents an equatorially symmetric distribution and explains approximately 70% of the variance. The combined ascending branch of this mode is located at the equator, and the two descending branches are located at about 30° in both hemispheres (Figures 5f–5j). The seasonal evolution of this mode's PC displays a sinusoidal variation, which is similar to that of HEA but with a smaller amplitude (Figure 6b). A further comparison among the various reanalyses indicates that despite the strong consistencies in the spatial and explained variance of the principal modes for both HEA and HES, the intensity of EOF1 in NCEP1 and NCEP2 is larger than in the other three data sets (i.e., ERA, JRA, and CFSR). Furthermore, the peak value of the HES PC occurs in December in NCEP1 but in April for the other four reanalyses. In fact, the climatological HC is an equatorially asymmetric structure in December (figure not shown), which implies that the equatorially symmetric component is weak at this time. By contrast, the climatological HC is approximately equatorially symmetric in April (figure not shown), indicating that the equatorially symmetric component is relatively strong at this time. Therefore, the discussion above indicates that there is some degree of limitation associated with the NCEP1 data set with respect to depicting the seasonal evolution of HES.

As for the zonal mean SST, since the calculation of asymmetric and symmetric components is based on the position of equator, the value of SEA at the equator is zero no matter in which season. The distribution of SES is mirrored with the equator, with equivalent peak in each hemisphere, but with amplitude changes during the seasonal cycle (figures not shown). The EOF1 of SEA displays an equatorially asymmetric structure, with positive values in the SH but negative values in the NH (Figure 7a), and explains around 98% of the variance. The PC of this mode varies sinusoidally along with the seasonal march (Figure 7b). EOF1 of SES shows an equatorially symmetric meridional distribution (Figure 7c). The amplitude of this mode's PC is much weaker than that of SEA (Figure 7d) and parallels the smaller amplitude of the HES PC. The correlation coefficients of the corresponding PCs for HEA and SEA, and HES and SES based on the different reanalyses, are all greater than 0.9. These high correlations indicate that the variations in HEA are closely linked to SEA and the variations in HES are connected with SES [*Feng and Li*, 2013].

On the other hand, it is seen that PC1 of HES peaks around April during boreal spring but peaks around August instead of October (Figure 6). The same interhemispheric asymmetry exists for SES. This may due to the nonlinear response of HC to SST [e.g., *Plumb and Hou*, 1992; *Zheng*, 1998; *Fang and Tung*, 1999; *Bordoni and Schneider*, 2010] and the active Asian summer monsoonal circulation [*Schneider and Bordoni*, 2008]. This point is verified by the significant relationship between the PCs of HES and SEA. However, not the case for that of the HEA and SES, it is possible that the peak in HES during August is due to the peak in

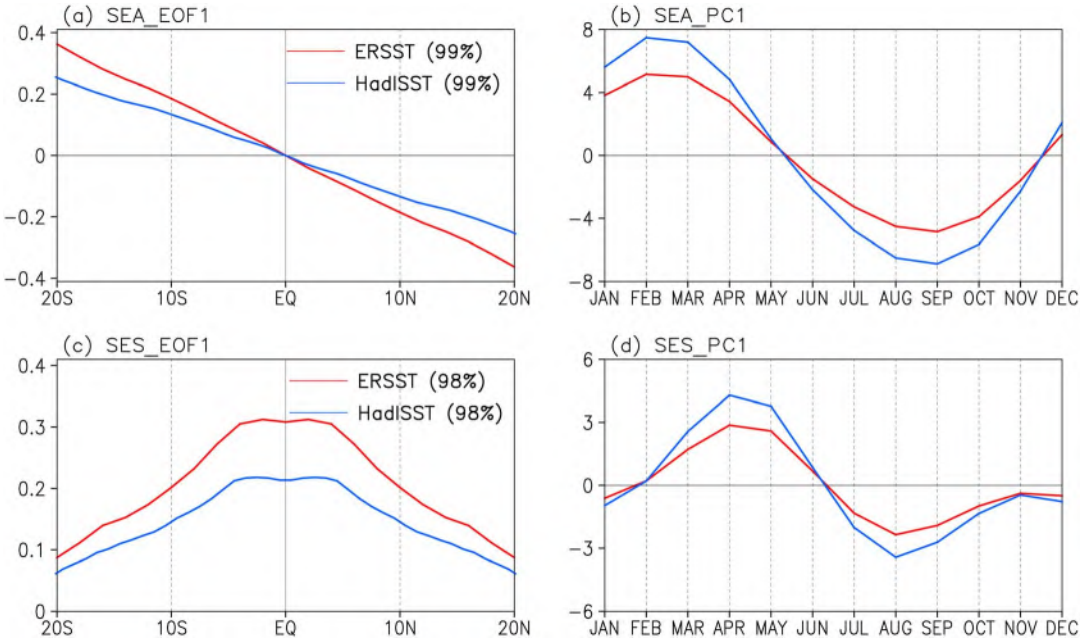

Figure 7. (a) EOF1 of the equatorially asymmetric part of SST during the seasonal cycle and (b) time series of EOF1 of the equatorially asymmetric part of SST. (c and d) As in Figures 7a and 7b but for the result of the equatorially symmetric part of SST. The red and blue lines indicate based on the ERSST and HadISST data, respectively.

SEA, corresponding to a nonlinear response of HC to SST. Moreover, considering that the SST shows strong persistence and memory, it has a possibility that the peak in SES during October is associated with that during August.

To this point, it is of interest to consider whether there are any differences between the responses of HES to SES and HEA to SEA, and if so, to what extent? The scatterplots of the first PCs of HEA against SEA, as well as for HES against SES, are presented in Figures 8 and 9. HEA and SEA, and HES and SES, are closely linearly correlated as mentioned above. However, the response of HEA to SEA consistently differs from that of HES to SES across the five reanalyses (i.e., NCEP1, NCEP2, JRA, ERA, and CFSR). For both the ERSST and HadISST data sets, the responses of HEA and HES to SST variations of equal amplitude in SEA and SES are significantly different (Table 1). The ratio of the responses of HEA to SEA, and HES to SES, is roughly 4:1 for the NCEP2, ERA, JRA, and CFSR reanalyses but is larger (~8:1) for the NCEP1 reanalysis. As discussed above, NCEP1 shows evident shortcomings in depicting the seasonal evolution of HES. Thus, the result based on NCEP1 is not included in the following analysis. On the other hand, although the exact values of the ratios vary across the reanalyses, the relative difference between the maximum (minimum) and the mean of the ratios is within 18%. This suggests that it is reasonable to take the average value of the ratio from the various reanalyses. That is, the response of HEA to SEA is approximately four times greater than that of HES to SES, even though the magnitude of the thermal forcing is the same. This analysis explains why the equatorially asymmetric mode dominates the variability of the seasonal cycle HC. That is, the response of the equatorially asymmetric circulation to the same magnitude of SST forcing is much greater than that of the equatorially symmetric circulation, which results in a much larger amplitude for the equatorially asymmetric than for the equatorially symmetric component. However, the amplitudes of the SEA and SES are equivalent (Figure 7b versus Figure 7d). These two aspects together contribute to the maintenance of the equatorially asymmetric mode.

To be noted is that previous study explored the response of zonally symmetric atmosphere to thermal forcing and found that there is a threshold behavior based on the inviscid steady state theory [e.g., *Plumb and Hou*, 1992; *Zheng*, 1998; *Bordoni and Schneider*, 2010]. Namely, atmosphere adopts a nonlinear response to the forcing. The difference between the result here and previous studies is mainly due to (1) different timescales focused: the thermal forcing in the previous studies is located in the subtropics [*Plumb and Hou*, 1992; *Fang and Tung*, 1999; *Zheng*, 1998], and the adjustment time for an axially symmetric model to obtain a steady state is on the order of 100 days or even longer than the seasonal timescale [*Fang and Tung*, 1999].

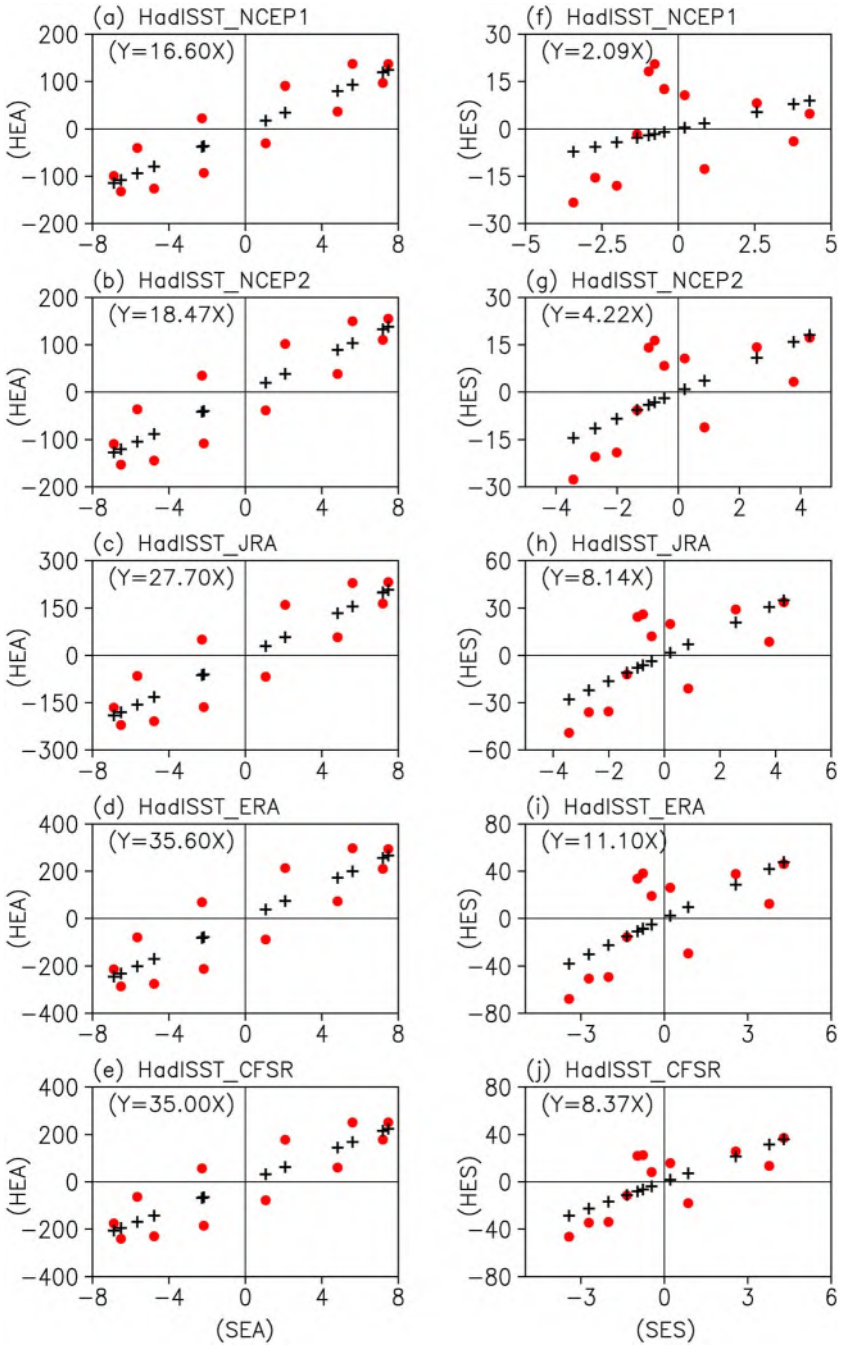

Figure 8. (a–e) Scatterplot of the first PC of the equatorially asymmetric part of SST against the first PC of the equatorially asymmetric part of the HC based on HadISST (red dots) and their linear fit (black crosses). (f–j) As in Figures 8a–8e but for the scatterplot of the first PC of the equatorially symmetric part of SST against the first PC of the equatorially symmetric part of the HC.

However, the heating varies on a seasonal cycle in the atmosphere. (2) The difference in forcing: as to the response of HES to SES, the maximum forcing is around the equator whereas displaced sufficiently far away from the equator [*Walker and Schneider*, 2006]. And to the response of HEA to SEA, the forcing is equivalent to the solstice forcing which is beyond the threshold. Both of the heating situations are dissimilar to the previous works. On the other hand, although the linear response of the HC to SST explains a large portion of the variance of HC, it is also found that the variation of HES is also closely linked with the variation of SEA, however not the case for that of SES and HEA. This point is consistent with

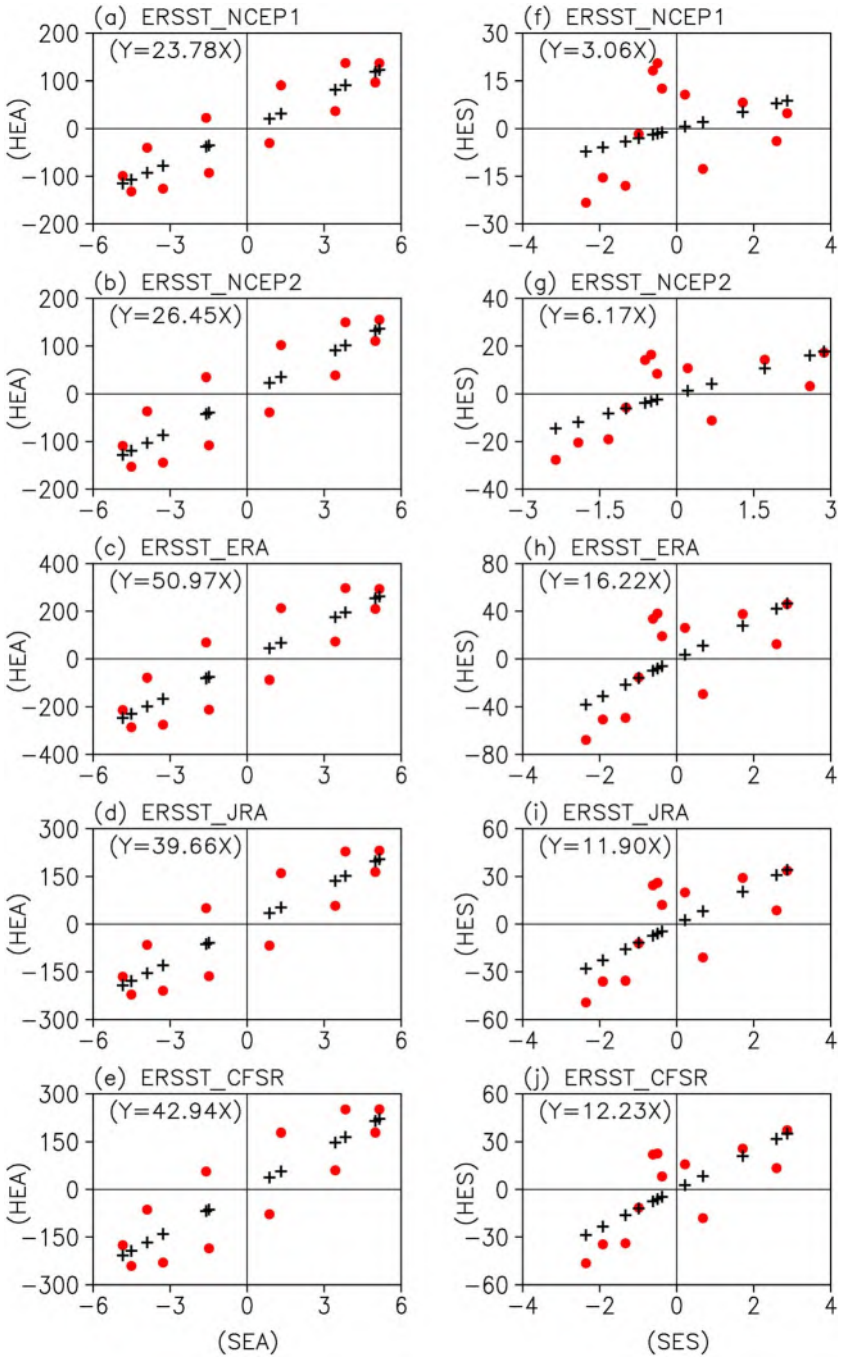

Figure 9. As in Figure 8 but based on ERSST.

previous studies; for instance, a heating off the equator contributes to both the equinox regime and solstice regime as suggested [*Walker and Schneider*, 2005, 2006].

5. Differing the Responses of the HC to SSTs Between the Seasonal Cycles and Interannual

Our previous work had discussed the contrasting responses of the HC to different SST meridional structures but concentrated on the interannual timescale over the period of 1948–2013 [*Feng et al.*, 2016b]. It is found that the response ratio of HEA to SEA is five times than that of the HES to SES at the interannual scale.

Table 1. Regression Coefficients of the HEA's (HES's) PC With Respect to SEA's (SES's) PC and Their Ratio Calculated Using the Various Reanalysis Data Sets

	ERSST			HadISST		
	ASY	SYM	Ratio	ASY	SYM	Ratio
NCEP1	23.78	3.06	7.77	16.60	2.09	7.94
NCEP2	26.45	6.17	4.29	18.47	4.22	4.38
ERA	50.97	16.22	3.14	35.60	11.10	3.18
JRA	39.66	11.90	3.33	27.70	8.14	3.40
CFSR	42.94	12.23	3.51	30.00	8.37	3.58

The different response ratios of the HC to different SST meridional structures during the interannual and seasonal cycle highlight the following two points. (1) The PC1 of HEA associated with long-term interannual variations shows a strong decadal variation and is significantly correlated with the Pacific Decadal Oscillation (PDO) index. This suggests that the decadal signals may have an influence on the variation of HEA, and the signals from the extratropics may impact on the HEA. In fact, previous studies have already reported that the Atlantic Multidecadal Oscillation [*Mantsis and Clement*, 2009; *Guo et al.*, 2016] and PDO [*Allen et al.*, 2016; *Wang et al.*, 2016] influence the long-term variation of the HC. It will be interesting to examine further the possible role of the HEA in these reported relationships. On the other hand, for the seasonal cycle, the influences from other factors could largely be ignored, and the fundamental driver of the HC is the seasonal shift of the Sun. Bearing this in mind, we found that the response ratio of the HC to different SST meridional structures is correspondingly reduced compared with the result from the long-term variability. That is, the other factors (e.g., decadal signals) play an essential role in driving the long-term variations of the HC, in which strengthened the decadal variations of the HC. (2) Our analysis of the seasonal cycle more closely matches the theoretical deductions and numerical experiments of *Feng et al.* [2016b], which further establishes that the impacts of the decadal as well as the strong interannual signals of the HC are reduced significantly during the seasonal cycle. However, the uncertainties associated with the decadal variations in the current Coupled General Circulation Models contribute considerably to their limited simulation performance. Therefore, the results of this study provide a feasible approach by which we can quantitatively assess the reproduction of the direct response of the large-scale atmospheric circulation to the thermal structures without interference from the decadal and interannual variations.

6. Discussion and Conclusions

In this study, using multiple atmospheric and ocean reanalysis data sets for the last three decades, we have investigated the influence of the meridional structure of SST on the HC, with a focus on the seasonal cycle. We decomposed the variations of the HC and SST into two components: the equatorially symmetric variations (i.e., HES and SES) and the equatorially asymmetric variations (i.e., HEA and SEA), to investigate the spatial and temporal characteristics of the HC and tropical SST during the seasonal cycle. We found that the response amplitude in HEA and SEA are much larger than those in HES and SES and demonstrated that the variations in the climatological HC are driven mainly by the variability of the equatorially asymmetric component. These results indicated that the variations of HEA are closely linked to those of SEA, and the variations of HES are linked to those of SES. Moreover, we found that the responses of HEA and HES to SST variations are distinct. Various reanalysis data sets consistently indicated that the disturbances of the same magnitude in SEA and SES are associated with different responses in the HC, and the response to SEA is about four times larger than that to SES. Our results provided a plausible explanation for the dominance of the equatorially asymmetric mode of the climatological HC during the seasonal cycle, because although the amplitudes of SEA and SES are equivalent, the response of HEA to SEA is much greater than that of HES to SES, leading to a much larger amplitude of the equatorially asymmetric variation of the HC. This relationship contributes to the formation of the dominant equatorially asymmetric mode during the seasonal cycle.

Moreover, the PC of SES exhibits a semiannual cycle (Figures 8f–8j and 9f–9j), and a similar result occurs when the semiannual cycle of SST is removed (figures not shown). Furthermore, although the phase transition timing of HES and SES is not simultaneous, but has a 1 month lag relative to the SES, a further examination of the relationship, as well as the response of HC to SST, was performed but with a 1 month lag in the SES, and it is found that the response differences as described above remain (figures not shown). This point further supported our interpretation of these results and indicates the reliability of the analysis presented in this study. In addition, we found that the NCEP1 reanalysis exhibits certain limitations in depicting the seasonal cycle of

the HES component, and NCEP1 may not be appropriate for the analysis of the long-term variability of the HC. For example, it has been reported that the long-term trend of NCEP1 is stronger [*Wu and Xie*, 2003], and the HC associated with NCEP1 is stronger than the observations [*Waliser et al.*, 1999], and also that the amplitude of the SH cell during the boreal summer is too low [*Stachnik and Schumacher*, 2011]. However, we focused on the seasonal cycle after 1979 in this study, which corresponds to the period when ground-based observations, along with satellite-based measurements, substantially improved the temporal and spatial sampling and reliability of the reanalysis products. Consequently, the ratio of the responses of HEA to SEA against HES to SES is exaggerated in the NCEP1 reanalysis compared with the other four reanalyses. However, we do not know the cause of this limitation and did not provide a full comparison across the available reanalyses during the seasonal march in portraying the characteristics of the HC in this study. Future work regarding this aspect will be needed to assess the possible causes of the uncertainties.

Meanwhile, using idealized experiments with a climate model, *Clement* [2006] found that ocean heat transport plays an important role in influencing the structure and intensity of the seasonal HC, and the results of this previous study suggested that both the oceanic and atmospheric processes, as well as their interactions, should be considered when studying the variability of the HC. Moreover, the response of the HC to SST involves complex physical processes, including possible roles for eddies, static stability, and stratification. Therefore, it is worth examining further their potential role in determining the impacts of the meridional structures of SST on the equatorially asymmetric and symmetric variations of the HC. This would help us to develop a more complete understanding of the HC and may provide a possible physical mechanism to explain how the influence of ocean processes is passed onto the HC. Moreover, although the decomposition method is linear, the response of the HC to SST cannot be interpreted as a solely linear process as reported. The correlations between the HEA and SEA, as well as between the HES and SES, are greater than 0.9 across the different data sets, suggesting that the linear response counts for a relatively large proportion of the variance. Therefore, the nonlinear response of the HC to SST was not investigated in this study.

Further, as indicated, the HC adopts the angular momentum conservation regime during solstice seasons (i.e., being equatorially asymmetric) and the eddy-mediated regime during equinox seasons (i.e., being equatorially symmetric) [e.g., *Walker and Schneider*, 2005; *Schneider and Bordoni*, 2008]. Therefore, it is of interest to investigate which regime does the equatorially asymmetric/symmetric variations follow and their relative roles in determining the variations of the equatorially asymmetric and symmetric HC. Besides, we highlight the different response amplitude of HC to different SST meridional structures; however, why does their response exhibit such differences and what is the involved physical process and feedback mechanisms. These questions warrant further work and left as open question.

Finally, our results based on the seasonal cycle differ somewhat from those that focused on long-term variations, for which it was found that the ratio of the responses between the equatorially asymmetric and symmetric components is about 5 [*Feng et al.*, 2016b]. This difference implies that the response of HEA and HES to SST is not constant and may vary with the timescale analyzed or possibly with the season. Therefore, we suggest examining whether the responses differ in each season and also a further exploration of the underlying mechanism that drives the differing responses. These problems warrant further examination and will be the focus of future studies.

Acknowledgments
The author Juan Feng acknowledges helpful discussions with Fred Kucharski and In-Sik Kang during her visit to the Abdus Salam International Centre for Theoretical Physics (ICTP). We thank three anonymous referees, whose comments improved the paper. This work was jointly supported by the Ministry of Science and Technology National Key Research and development Projects of China (2016YFA0601801), National Natural Science Foundation of China (41475076), and SOA Program on Global Change and Air-Sea interactions (GASI-IPOVAI-03). The NCEP/NCAR, NCEP/DOE Reanalysis and ERSST reanalyses were obtained from NOAA and are available at http://www.esrl.noaa.gov/psd/data/gridded/. The ERA-Interim reanalysis was obtained from http://apps.ecmwf.int/datasets/. The JRA reanalysis is available online at http://jra.kishou.go.jp/JRA-55/index_en.html. The CFSR reanalysis is available online at http://cfs.ncep.noaa.gov/cfsr/. The HadISST data set was obtained from the UK Met Office Hadley Centre and is available online at http://www.metoffice.gov.uk/hadobs/hadisst/data/download.html.

References

Adam, O., T. Schneider, and N. Harnik (2014), Role of changes in mean temperatures versus temperature gradients in the recent widening of the Haley circulation, *J. Clim.*, *27*, 7450–7461.

Allen, R. J., J. R. Norris, and M. Kovilakam (2016), Influence of anthropogenic aerosols and the Pacific decadal oscillation on tropical belt width, *Nat. Geosci.*, *7*, 270–274, doi:10.1038/NGE02091.

An, Z. S., et al. (2015), Global monsoon dynamics and climate change, *Annu. Rev. Earth Planet. Sci.*, *43*, 29–77.

Byrne, M. P., and T. Schneider (2016), Narrowing of the ITCZ in a warming climate: Physical mechanisms, *Geophys. Res. Lett.*, *43*, 11,350–11,357, doi:10.1029/2016GL070396.

Bordoni, S., and T. Schneider (2010), Regime transitions of steady and time-dependent Hadley circulations: Comparison of axisymmetric and eddy-permitting simulations, *J. Atmos. Sci.*, *67*, 1643–1654.

Clement, A. C. (2006), The role of the ocean in the seasonal cycle of the Hadley circulation, *J. Clim.*, *63*, 3351–3365.

Dee, D. P., et al. (2011), The ERA-Interim reanalysis: Configuration and performance of the data assimilation system, *Q. J. R. Meteorol. Soc.*, *137*(656), 553–597.

Diaz, H. F., and B. Bradley (2004), *The Hadley Circulation: Present, Past and Future*, Kluwer Acad., Netherlands.

Dima, I. M., and M. J. Wallace (2003), On the seasonality of the Hadley cell, *J. Atmos. Sci.*, *60*, 1522–1526.

Fang, M., and K. K. Tung (1999), Time-dependent nonlinear Hadley circulation, *J. Atmos. Sci.*, *56*, 1797–1807.

Feng, J., and J. P. Li (2013), Contrasting impacts of two types of ENSO on the boreal spring Hadley circulation, *J. Clim.*, *26*, 4773–4789.
Feng, J., J. P. Li, and F. Xie (2013), Long-term variation of the principal mode of boreal spring Hadley circulation linked to SST over the Indo-Pacific warm pool, *J. Clim.*, *26*, 532–544.
Feng, J., J. L. Zhu, and F. Li (2016a), Climatological vertical features of Hadley circulation depicted by the NCEP/NCAR, ERA40, NCEP-DOE, JRA25, EAR-Interim, and CFSR reanalyses, *SOLA*, *12*, 237–241, doi:10.2151/sola.2016-047.
Feng, J., J. P. Li, F.-F. Jin, Z. Liu, X. Nan, and Y. Guo (2016b), Contrasting responses of the Hadley circulation to equatorially asymmetric and symmetric meridional sea surface temperature structures, *J. Clim.*, *29*, 8949–8963.
Feng, R., J. P. Li, and J. C. Wang (2011), Regime change of the boreal summer Hadley circulation and its connection with the tropical SST, *J. Clim.*, *24*, 3867–3877.
Fu, Q., C. M. Johanson, J. M. Wallace, and T. Reichler (2006), Enhanced mid-latitude tropospheric warming in satellite measurements, *Science*, *312*, 1179.
Guo, Y. P., J. P. Li, J. Feng, F. Xie, C. Sun, and J. Zheng (2016), The multidecadal variability of the asymmetric mode of the boreal autumn Hadley circulation and its link to the Atlantic Multidecadal Oscillation, *J. Clim.*, *29*, 5625–5641.
Holton, J. R. (1994), *An Introduction to Dynamic Meteorology*, Academic Press, New York.
Hou, A. Y. (1998), Hadley circulation as a modulator of the extratropical climate, *J. Clim.*, *55*, 2437–2457.
Hou, A. Y., and R. S. Lindzen (1992), The influence of concentrated heating on the Hadley circulation, *J. Atmos. Sci.*, *49*(14), 1233–1241.
Hu, Y. Y., and Q. Fu (2007), Observed poleward expansion of the Hadley circulation since 1979, *Atmos. Chem. Phys.*, *7*, 5229–5236.
Hudson, R. D., M. F. Andrade, M. B. Follette, and A. D. Frolov (2006), The total zone field separated into meteorological regimes—Part II: Northern Hemisphere mid-latitude total ozone trends, *Atmos. Chem. Phys.*, *6*, 5183–5191.
Johanson, C., and Q. Fu (2009), Hadley cell widening: Model simulations versus observations, *J. Clim.*, *22*, 2713–2725.
Kalnay, E., et al. (1996), The NCEP/NCAR 40-Year Reanalysis Project, *Bull. Am. Meteorol. Soc.*, *77*, 437–472.
Kanamitsu, M., W. Ebisuzaki, J. Woollen, S. K. Yang, J. J. Hnilo, M. Fiorino, and G. L. Potter (2002), NCEP-DOE AMIP-II Reanalysis (R-2), *Bull. Am. Meteorol. Soc.*, *83*, 1631–1643.
Li, J. P., and J. Feng (2017), Tropical large-scale atmospheric interaction in association with subtropical aridity trend, in *Aridity Trend in Northern China*, edited by C. B. Fu and H. T. Mao, 320 pp., World Sci. Co. Pte Ltd, Singapore.
Lindzen, R. S. (1994), Climate dynamics and global change, *Annu. Rev. Fluid Mech.*, *26*, 353–378.
Lindzen, R. S., and A. Y. Hou (1988), Hadley circulations for zonally averaged heating centered off the equator, *J. Atmos. Sci.*, *45*, 2416–2427.
Lindzen, R. S., and S. Nigam (1987), On the role of sea surface temperature gradients in forcing low-level winds and convergence in the tropics, *J. Atmos. Sci.*, *44*, 2418–2436.
Ma, J., and J. P. Li (2008), The principal modes of variability of the boreal winter Hadley cell, *Geophys. Res. Lett.*, *35*, L01808, doi:10.1029/2007GL031883.
Mantsis, D. F., and A. C. Clement (2009), Simulated variability in the mean atmospheric meridional circulation over the 20th century, *Geophys. Res. Lett.*, *36*, L06704, doi:10.1029/2008GL036741.
Melice, J. L., and J. Servain (2003), The tropical Atlantic meridional SST gradient index and its relationships with the SOI, NAO, and Southern Ocean, *Clim. Dyn.*, *20*, 447–464.
Mitas, C. M., and A. Clement (2005), Has the Hadley cell been strengthening in recent 329 decades?, *Geophys. Res. Lett.*, *32*, L03809, doi:10.1029/2004GL021765.
Nguyen, H., A. Evans, C. Lucas, I. Smith, and B. Timbal (2013), The Hadley circulation in reanalyses: Climatology, variability, and change, *J. Clim.*, *26*, 3357–3376.
Numaguti, A. (1994), Dynamics and energy balance of the Hadley circulation and the tropical precipitaton zones. Part II: Sensitivity to meridional SST distribution, *J. Atmos. Sci.*, *52*(8), 1128–1141.
Onogi, K., et al. (2005), JRA-25: Japanese 25-year re-analysis project—Progress and status, *Q. J. R. Meteorol. Soc.*, *131*, 3259–3268.
Parfitt, R., A. Czaja, S. Minobe, and A. K. Yoshida (2017), The atmospheric frontal response to SST perturbations in the Gulf Stream region, *Geophys. Res. Lett.*, *43*, 2299–2306, doi:10.1002/2016GL067723.
Peixoto, J. P., and A. H. Oort (1992), *Physics of Climate*, 520 pp., Am. Inst. of Phys., New York.
Plumb, R. A., and A. Y. Hou (1992), The response of a zonally symmetric atmosphere to subtropical thermal forcing: Threshold behavior, *J. Atmos. Sci.*, *49*, 1790–1799.
Previdi, M., and B. G. Liepert (2007), Annular modes and Hadley cell expansion under global warming, *Geophys. Res. Lett.*, *34*, L22701, doi:10.1029/2007GL031243.
Quan, X. W., H. F. Diaz, and M. P. Hoerling (2004), Change in the tropical Hadley cell since 1950, in *Hadley Circulation: Present, Past and Future*, edited by H. F. Diaz and R. S. Bradley, pp. 85–120, Springer, New York.
Rayner, N. A., D. Parker, E. Horton, C. K. Folland, L. V. Alexander, D. P. Rowell, E. C. Kent, and A. Kaplan (2003), Global analyses of sea surface temperature, sea ice, and night marine air temperature since the late nineteenth century, *J. Geophys. Res.*, *108*(D14), 4407, doi:10.1029/2002JD002670.
Rind, D., and W. B. Rossow (1984), The effects of physical processes on the Hadley circulation, *J. Atmos. Sci.*, *41*(4), 479–507.
Saha, S., et al. (2010), The NCEP climate forecast system reanalysis, *Bull. Am. Meteorol. Soc.*, *91*(8), 1015–1057.
Schneider, E., and R. S. Lindzen (1977), Axially symmetric steady state models of the basic state of instability and climate studies. Part I: Linearized calculations, *J. Atmos. Sci.*, *34*, 253–279.
Schneider, T., and S. Bordoni (2008), Eddy-mediated regime transitions in the seasonal cycle of a Hadley circulation and implications for monsoon dynamics, *J. Atmos. Sci.*, *65*, 915–934.
Seidel, D. J., and R. J. Randel (2007), Recent widening of the tropical belt: Evidence from tropopause observations, *J. Geophys. Res.*, *112*, D20113, doi:10.1029/2007JD008861.
Seidel, D. J., Q. Fu, W. J. Randel, and T. J. Reichler (2007), Widening of the tropical belt in changing climate, *Nat. Geosci.*, *1*, 21–24, doi:10.1038/ngeo.2007.38.
Smith, T. M., R. W. Reynolds, T. C. Peterson, and J. Lawrimore (2008), Improvements to NOAA's historical merged land-ocean surface temperature analysis (1880-2006), *J. Clim.*, *21*, 2283–2296.
Stachnik, J. P., and C. Schumacher (2011), A comparison of the Hadley circulation in modern reanalyses, *J. Geophys. Res.*, *116*, D22102, doi:10.1029/2011JD016677.
Su, H., J. H. Jiang, C. X. Zhai, T. J. Shen, J. D. Neelin, G. L. Stephens, and Y. L. Yung (2014), Weakening and strengthening structures in the Hadley circulation change under global warming and implications for cloud response and climate sensitivity, *J. Geophys. Res. Atmos.*, *119*, 5787–5805, doi:10.1002/2014JD021642.

Su, H., et al. (2017), Tightening of tropical ascent and high clouds key to precipitation change in a warmer climate, *Nat. Commun.*, *8*, 15771, doi:10.1038/ncomms15771.

Waliser, D. E., A. Shi, J. R. Lanzante, and A. H. Oort (1999), The Hadley circulation: Assessing NCEP/NCAR reanalysis and sparse in-situ estimates, *Clim. Dyn.*, *15*, 719–735.

Walker, C. C., and T. Schneider (2005), Response of idealized Hadley circulations to seasonally varying heating, *Geophys. Res. Lett.*, *32*, L06813, doi:10.1029/2004GL022304.

Walker, C. C., and T. Schneider (2006), Eddy influences on Hadley circulations: Simulations with an idealized GCM, *J. Atmos. Sci.*, *63*, 3333–3350.

Wang, W., K. Matthes, N. E. Omrani, and M. Latif (2016), Decadal variability of tropical tropopause temperature and its relationship to the Pacific Decadal Oscillation, *Sci. Rep.*, *6*, 29637, doi:10.1038/srep29537.

Wodzicki, K. R., and A. D. Rapp (2016), Long-term characterization of the Pacific ITCZ using TRMM, GPCP, and ERA-Interim, *J. Geophys. Res. Atmos.*, *121*, 3153–3170, doi:10.1002/2015JD024458.

Wu, R., and S. P. Xie (2003), On equatorial Pacific surface wind changes around 1977: NCEP–NCAR reanalysis versus COADS observations, *J. Clim.*, *16*, 167–173.

Zheng, X. Y. (1998), The response of a moist zonally symmetric atmosphere to subtropical surface temperature perturbation, *Q. J. R. Meteorol. Soc.*, *124*, 1209–1226.